Safety, Dosimetry, and Tumor Detection Ability of ^{68}Ga-NOTA-AE105: First-in-Human Study of a Novel Radioligand for uPAR PET Imaging

Dorthe Skovgaard*[1], Morten Persson*[2], Malene Brandt-Larsen[1], Camilla Christensen[1], Jacob Madsen[1], Thomas Levin Klausen[1], Søren Holm[1], Flemming Littrup Andersen[1], Annika Loft[1], Anne Kiil Berthelsen[1], Helle Pappot[3], Klaus Brasso[4], Niels Kroman[5], Liselotte Højgaard[1], and Andreas Kjaer[1]

[1]*Department of Clinical Physiology, Nuclear Medicine & PET and Cluster for Molecular Imaging, Rigshospitalet and University of Copenhagen, Copenhagen, Denmark;* [2]*Curasight, Copenhagen, Denmark;* [3]*Department of Oncology, Rigshospitalet, Copenhagen, Denmark;* [4]*Department of Urology, Copenhagen Prostate Cancer Center, Rigshospitalet, Copenhagen, Denmark; and* [5]*Department of Plastic Surgery, Breast Surgery and Burns Treatment, Rigshospitalet, Copenhagen, Denmark*

The overexpression of urokinase-type plasminogen activator receptors (uPARs) represents an established biomarker for aggressiveness in most common malignant diseases, including breast cancer (BC), prostate cancer (PC), and urinary bladder cancer (UBC), and is therefore an important target for new cancer therapeutic and diagnostic strategies. In this study, uPAR PET imaging using a ^{68}Ga-labeled version of the uPAR-targeting peptide (AE105) was investigated in a group of patients with BC, PC, and UBC. The aim of this first-in-human, phase I clinical trial was to investigate the safety and biodistribution in normal tissues and uptake in tumor lesions. **Methods:** Ten patients (6 PC, 2 BC, and 2 UBC) received a single intravenous dose of ^{68}Ga-NOTA-AE105 (154 ± 59 MBq; range, 48–208 MBq). The biodistribution and radiation dosimetry were assessed by serial whole-body PET/CT scans (10 min, 1 h, and 2 h after injection). Safety assessment included measurements of vital signs with regular intervals during the imaging sessions and laboratory blood screening tests performed before and after injection. In a subgroup of patients, the in vivo stability of ^{68}Ga-NOTA-AE105 was determined in collected blood and urine. PET images were visually analyzed for visible tumor uptake of ^{68}Ga-NOTA-AE105, and SUVs were obtained from tumor lesions by manually drawing volumes of interest in the malignant tissue. **Results:** No adverse events or clinically detectable pharmacologic effects were found. The radioligand exhibited good in vivo stability and fast clearance from tissue compartments primarily by renal excretion. The effective dose was 0.015 mSv/MBq, leading to a radiation burden of 3 mSv when the clinical target dose of 200 MBq was used. In addition, radioligand accumulation was seen in primary tumor lesions as well as in metastases. **Conclusion:** This first-in-human, phase I clinical trial demonstrates the safe use and clinical potential of ^{68}Ga-NOTA-AE105 as a new radioligand for uPAR PET imaging in cancer patients.

Key Words: molecular imaging; oncology; general; PET/CT; ^{68}Ga-NOTA-AE105; first in humans; phase I; uPAR PET

J Nucl Med 2017; 58:379–386
DOI: 10.2967/jnumed.116.178970

The urokinase-type plasminogen activator receptor (uPAR) is a cell membrane protein involved in extracellular matrix degradation. Besides regulating proteolysis, uPAR also activates many intracellular signaling pathways that promote cell motility, invasion, and proliferation through cooperation with transmembrane receptors. In normal tissues, uPAR expression is limited. However, in cancer uPAR is frequently overexpressed, for example, in urinary bladder cancer (UBC), uPAR immunoreactivity is detected in 96% of the neoplasias at the invasive front (*1*), and in more than 500 breast cancer (BC) patients studied only 2% had uPAR levels below the detection limit (*2*). Importantly, high uPAR expression is associated with cancer invasion and metastases. Accordingly, uPAR represents an established biomarker for aggressive disease and poor prognosis in a variety of human cancers, including the most common malignant diseases, such as BC, colorectal cancer, lung cancer, UBC, and prostate cancer (PC) (*1,3–11*).

These observations highlight and support that noninvasive imaging of uPAR in cancer tissue could become a clinically relevant diagnostic and prognostic imaging biomarker with the possibility of distinguishing indolent tumors from the invasive phenotype.

Accordingly, we have for several years focused on development of radioligands based on the high-affinity peptide antagonist AE105 for PET imaging of uPAR expression (*12–17*). We recently published results from a promising first-in-human study with ^{64}Cu-DOTA-AE105 showing high uptake in both primary tumor lesions and lymph node metastases paralleled with high uPAR expression in excised tumor tissue, thereby providing evidence for uPAR PET imaging in cancer patients (*4*). However, clinical translation of ^{64}Cu-based radioligands is hampered by limited availability and the necessity of a cyclotron facility to produce the PET isotopes. In line with this, the generator-based PET isotope ^{68}Ga has gained special attention because of its independence

Received May 31, 2016; revision accepted Aug. 18, 2016.
For correspondence or reprints contact: Andreas Kjaer, Department of Clinical Physiology, Nuclear Medicine & PET, KF-4012, Rigshospitalet, National University Hospital, Blegdamsvej 9, 2100 Copenhagen, Denmark.
E-mail: akjaer@sund.ku.dk
*Contributed equally to this work.
Published online Sep. 8, 2016.

of an onsite cyclotron and a half-life of 68 min, which matches well with the pharmacokinetics of peptides such as the AE105 (*18*). The goal of the present phase I study was to investigate the feasibility of ^{68}Ga-NOTA-AE105 for tumor imaging in humans. The primary aim was to evaluate the safety, pharmacokinetics, and internal radiation dosimetry of a single-dose injection of ^{68}Ga-NOTA-AE105 in cancer patients using PET/CT imaging. The secondary objective was to investigate the uptake in primary tumor lesions and potentially in metastases if present.

MATERIALS AND METHODS

Study Design

In this open-label phase I study, 10 patients with histopathologically confirmed PC (6 patients), BC (2 patients), or UBC (2 patients) were enrolled from May 2015 to July 2015 (Table 1). All patients gave written informed consent before inclusion. The study was approved by the Danish Health and Medicine Authority (EudraCT no. 2014-005522-35) and the Ethical Committee of the Capital Region of Denmark (protocol H-15002406). The study was registered at ClinicalTrials.gov (NCT02437539) and was performed in accordance with the recommendation for Good Clinical Practice including independent monitoring by the Good Clinical Practice unit of the Capital Region of Denmark. All patients were injected intravenously with approximately 200 MBq of ^{68}Ga-NOTA-AE105 followed by sequential whole-body PET/CT scanning 10 min, 1 h, and 2 h after injection. The dose was chosen to provide adequate count statistics and based on preclinical data was projected to be well below the maximum acceptable radiation exposure and at the same level as ^{18}F-FDG PET scanning. In a subset of 6 patients (patients 4, 5, 6, 7, 8, and 10), blood was collected approximately 1, 5, 30, and 90 min after injection for pharmacokinetic analysis, including ligand stability. Urine was collected from 3 patients (patients 7, 8, and 10) during the test period. Safety measures included observation and systematic questions of subjective well-being and monitoring of heart rate and blood pressure with regular intervals before, during, and after the last image session (1 min, 10 min, 1 h, and 2 h after injection). Hematologic (hemoglobin, white blood cells, platelets), liver (alanine amino transferase, alkaline phosphatase, lactate dehydrogenase), and renal function (s-creatinine, glomerular filtration rate, sodium, potassium) were measured before radioligand administration, immediately after and on return to the hospital 3–21 d after the study day (Supplemental Fig. 1; supplemental materials are available at http://jnm.snmjournals.org). When available, preoperative biopsies or surgically excised primary tumor tissue and local lymph nodes were collected for target validation, demonstrating immunohistochemical expression of uPAR.

Production of ^{68}Ga-NOTA-AE105

NOTA-AE105 trifluoroacetate was obtained from ABX GmbH. ^{68}Ga (half-life = 68 min; maximum positron energy [$E_{max,\ \beta+}$] = 1.90 MeV [89%]) labeling of NOTA-AE105 trifluoroacetate was performed using a Modular-Lab Standard module (Eckert & Ziegler). The ^{68}Ge/^{68}Ga generator (IGG100; Eckert & Ziegler) was eluted with 6 mL of 0.1 M HCl. The eluate was concentrated on a Strata-XC cartridge and eluted with 700 μL of 0.82 M HCl/acetone (2:98). NOTA-AE105 (32 nmol), dissolved in 10 μL of dimethyl sulfoxide, was labeled in 500 μL of 0.7 M NaOAc buffer, pH 5.2, and 200 μL of 96% EtOH at room temperature for 12 min. The resulting product, ^{68}Ga-NOTA-AE105, was purified on a SepPak C18 light cartridge (Waters), eluted with 50% ethanol, and formulated with saline to a total volume of 7 mL.

For analysis, a high-performance liquid chromatograph (Ultimate 3000; Dionex) was used with a 2.6-μm, 100-Å, 50 × 4.6 mm C18 column (Kinetex) and with the ultraviolet and radiodetector connected in series. The mobile phases were eluent A, 10% MeCN in H_2O with 0.1% trifluoroacetic acid, and eluent B, 10% H_2O in MeCN with 0.1% trifluoroacetic acid. For thin-layer chromatography a ScanRam scanner and plates were used. The mobile phase was 77 g of ammonium acetate per liter in water/methanol (1:1). For gas chromatography, a Shimadzu GC2014 was used with a Zebron ZB-WAX 30 m × 0.53 mm × 1.00 μm column.

PET/CT Acquisition

All subjects fasted 6 h before injection of ^{68}Ga-NOTA-AE105. Two peripheral intravenous catheters were placed, 1 for radiotracer injection and 1 in the contralateral arm for withdrawal of blood samples and administration of CT contrast agent.

Data acquisition was performed using a PET/CT system (Biograph mCT; Siemens Medical Solutions) with an axial field of view of 216 mm. Emission scans were acquired 10 min, 1 h, and 2 h after intravenous administration of ^{68}Ga-NOTA-AE105 (≈200 MBq). Whole-body PET scans were obtained in 3-dimensional mode, with an acquisition time of 2 min per bed position. Attenuation- and scatter-corrected PET data were reconstructed iteratively using a 3-dimensional ordinary Poisson ordered-subset expectation-maximization algorithm including point-spread function and time-of-flight information (Siemens Medical Solutions); the settings were 2 iterations, 21 subsets, 2-mm gaussian filter, and a 400 × 400 matrix. Pixel size in the final reconstructed PET image was approximately 2 × 2 mm with a slice thickness of 2 mm. Due to artifacts, the halo effect on ^{68}Ga-NOTA-AE105 PET in the tissue surrounding the urinary bladder caused by the prompt γ of ^{68}Ga at 1,077 keV (brancing ratio of 3.2%) (*19*), all image data were also reconstructed using prompt γ-correction. A diagnostic CT scan was obtained before the 1-h PET scan, with a 2-mm slice thickness, 120 kV, and a quality reference of 225 mAs modulated by the Care Dose 4D automatic exposure control system (Siemens Medical Solutions). A low-dose CT scan, 2-mm slice thickness, 120 kV, and 40 mAs, was acquired before each of the 10-min and 2-h scans and used for attenuation correction. An automatic injection system was used to administer 75 mL of an iodine-containing contrast agent (Optiray 300; Covidien) with a scan delay of 60 s and flow rate of 1.5 mL/s, followed by an injection of 100 mL of NaCl with a flow rate of 2.5 mL/s. PET images in units of Bq/mL were used for quantitative analysis of tissue radioactivity concentrations for dosimetry purposes and for calculation of SUVs.

Plasma Pharmacokinetics and Urine Metabolite Analysis

The blood and urine samples were analyzed on a Dionex UltiMate 3000 column-switching high-pressure liquid chromatograph system with a Posi-RAM Module 4 as previously described (*4*). The mobile phase for the extraction step was 0.1% trifluoroacetic acid in H2O, whereas the analytic step was a gradient method with solvent A, 0.1% trifluoroacetic acid in MeCN: H2O 10:90, and solvent B, 0.1% trifluoroacetic acid in MeCN:H2O 90:10, both with a flow of 1.5 mL/min. The gradient was 0–6 min (extraction), 6–7 min 0%–10% B, 7–13 min 10%–65% B, 13–14 min 65%–10% B, 14–15 min 10% B.

Dosimetry

Dosimetry was based on the decay-uncorrected image sets from the 3 time points supplemented with sampled urine data (3 patients) as previously described (*4*). Briefly, cumulated activity for each patient and organ was determined by integration of time–activity curves based on an average of 3 spheric volumes of interest (VOIs) placed in all major organs defined on CT images using Mirada RTx (Mirada Medical). Individual urine excretion data were fitted to monoexponentials yielding the fraction of injected activity excreted and a biologic half-life of the process. All data were entered into OLINDA/EXM software (Vanderbilt University) to obtain corresponding estimates of organ-absorbed doses and effective dose. OLINDA's Voiding Bladder Model was used with fraction and half-life from the fitted urine data as input and an assumed bladder-voiding interval of 1 h.

TABLE 1
Patient Characteristics

Characteristic	Patient no.									
	1	2	3	4	5	6	7	8	9	10
Sex	Female	Male	Male	Male	Female	Male	Male	Male	Male	Male
Age (y)	51	70	74	67	28	71	57	52	66	74
Cancer type	Breast ductal carcinoma	Prostate	Prostate	Prostate	Breast ductal carcinoma	Bladder	Prostate	Prostate	Bladder	Prostate
Stage/grade	Grade III	cT3N0M0	cT3N0M0	cT3N0M0	Grade II	Disseminated disease—no residual lesions on treatment evaluation CT	Disseminated bone metastases, initially treated with local radiotherapy (2008)	Disseminated bone metastases at the time of diagnosis (2014)	Disseminated disease—2 liver metastases on treatment evaluation CT	cT3N0M0
Biomarker status	Estrogen-positive HER-2 negative	Gleason score 4 + 5, PSA 56	Gleason score 4 + 5, PSA 23	Gleason score 3 + 4, PSA 9	Estrogen-positive HER-2–positive	NA	PSA 128	PSA 11	NA	Gleason 4 + 5, PSA 8
Ongoing systemic therapies	No	No	No	No	No	Cisplatin and Gemxar (6 series)	Docetaxel (7 series)	Firmagon + Xgeva Docetaxel (6 series)	Cisplatin and Gemxar (6 series)	No
No. of d after PET scan before operation	5	9	2	14	2	NA	NA	NA	NA	20

HER-2 = human epidermal growth factor receptor 2; PSA = prostate-specific antigen; NA = not applicable.

Tumor Uptake by Visual Image Analysis and Activity Quantification

All image data were analyzed by a team consisting of a highly experienced certified specialist in nuclear medicine and a highly experienced certified specialist in radiology for the presence of lesions suggestive of cancer. Semiquantitative analyses of visually detectable tumor lesions were done by drawing spheric VOIs. Because of low counts, the image quality of the last scan (2 h after injection) was suboptimal for assessing tumor uptake, and therefore SUVs were calculated only from the generated VOIs for the first 2 PET scans (10 min and 1 h after injection) and parameterized as SUV_{mean} and SUV_{max}. In some cases, the standard PET reconstruction showed a reduced signal (halo effect) around the urinary bladder. The halo led to hampered tumor visualization and to underestimation of SUVs of both normal and tumor tissue. Therefore, all PET image data were reconstructed again using prompt γ-correction. The data were subsequently reanalyzed for tumor uptake by the same team of specialists, with more than 3 mo between interpretations, and the SUVs presented here were obtained from prompt γ-corrected images.

Collection of Tissue Samples and Immunohistochemistry of uPAR Expression

Surgical specimens of primary tumors and metastases were obtained from 2 BC patients undergoing surgical treatment subsequently to ^{68}Ga-NOTA-AE105 PET. The time interval between ^{68}Ga-NOTA-AE105 PET and surgery was 5 and 2 d, respectively. Four of the patients with locally advanced PC underwent lymphadenectomy before radiation therapy. None of these patients had lymph node metastases based on CT findings. Prostate tumor specimens were available from the preoperative prostate biopsies only (except from patient 5, for whom the initial biopsy was taken at a regional hospital and therefore not available). The specimens were placed in formalin. Sections were prepared with paraffin sections (2.5 μm thick), and a standard immunohistochemistry technique (avidin–biotin–peroxidase) was performed to visualize the immunostaining intensity and distribution of uPARs as previously described using the monoclonal antibody R^2 (*4*). In addition, hematoxylin and eosin staining was performed. The sections were visually evaluated for visible uPAR-positive staining and scored as either positive or negative.

Statistics

The significance of differences in vital signs and blood tests were evaluated using ANOVA. A P value of less than 0.05 was considered statistically significant.

RESULTS

Radiochemistry

All preparations complied with the specifications. The specifications and results of the ^{68}Ga-NOTA-AE105 preparations are given in Supplemental Table 1.

Patient Safety and Dosimetry

The administered mass of NOTA-AE105 was 13.6 ± 8.7 μg (range, 4.4–34.7 μg). The mean administered activity was 154 ± 59 MBq (range, 48–208 MBq). None of the patients experienced infusion-related reactions or adverse events. There were no clinically detectable pharmacological effects of ^{68}Ga-NOTA-AE105 and no changes in general well-being or vital signs (Supplemental Table 2). No acute or long-term effects on blood parameters or organ (liver and kidney) functions were found using standard biochemical parameters before and after participation in this study (Supplemental Fig. 1). The dose calculations yielded an effective dose of 0.015 mSv/MBq (Table 2). The bladder was the organ with the highest absorbed dose (0.131 mGy/MBq), followed by the kidneys (0.070 mGy/MBq).

Biodistribution, Pharmacokinetics, and Image Quality

A characteristic imaging series, illustrating biodistribution at 10 min, 1 h, and 2 h after injection, is shown in Figure 1. The excretion route appeared to be mainly through the kidneys with no or little excretion through the hepatobiliary/gastrointestinal tract. Persistently, there was a relatively high but decreasing blood-pool activity, and virtually no activity was found in the brain, lung, bone, and muscle.

Six of 10 patients (patients 4, 5, 6, 7, 8, and 10) in the study were used for investigating the plasma pharmacokinetics of ^{68}Ga-NOTA-AE105. A plasma half-life of 8.5 min was found. Only intact ^{68}Ga-NOTA-AE105 and no major metabolites were detected in plasma or urine (Supplemental Fig. 2).

Tumor Uptake of ^{68}Ga-NOTA-AE105 and Ex Vivo Target Validation

The secondary objective of this study was to investigate the uptake of ^{68}Ga-NOTA-AE105 in malignant tissue in BC, PC, and UBC. Patient-specific clinical information and imaging findings are detailed in Table 3.

TABLE 2
uPAR PET Dosimetry

Organ/tissue	Mean absorbed dose (mGy/MBq)
Adrenals	0.0118
Brain	0.00193
Breast	0.00599
Gallbladder wall	0.00838
Lower large intestine wall	0.00895
Small intestine	0.0177
Stomach wall	0.0114
Upper large intestine wall	0.0129
Heart wall	0.021
Kidneys	0.0699
Liver	0.0134
Lungs	0.00662
Muscle	0.00669
Ovaries	0.00909
Pancreas	0.012
Red marrow	0.00869
Osteogenic cells	0.0137
Skin	0.00564
Spleen	0.0146
Testes	0.00736
Thymus	0.00677
Thyroid	0.0128
Urinary bladder wall	0.131
Uterus	0.0109
Total body	0.00924
Effective dose (mSv/MBq)	0.0153

Mean absorbed dose per unit administered (mGy/MBq) of major organs were derived from serial whole-body PET scans acquired 10 min and 1 and 2 h after injection of ^{68}Ga-NOTA-AE105 using VOI-based time–activity data.

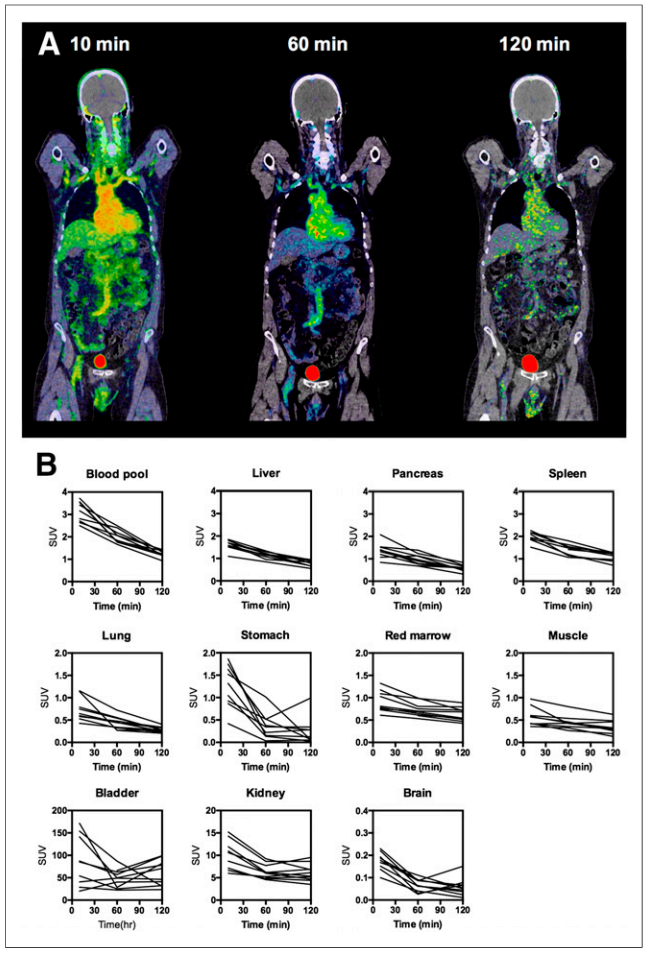

FIGURE 1. Whole-body distribution and SUV in major organs after injection of ^{68}Ga-NOTA-AE105. (A) Maximum-intensity-projection PET images at 10 min, 1 h, and 2 h after injection of ^{68}Ga-NOTA-AE105 (patient 2). Highest accumulation of activity was in kidneys and bladder. (B) Decay-corrected SUVs in blood and major organs plotted individually for n = 10 patients. For each patient, regions of interest were drawn on selected organ of interest at all 3 consecutive PET scans.

BC

Two BC patients were included before surgical intervention (patients 1 and 6). On qualitative image analysis, primary tumor uptake was clearly visualized already at the first (10 min) and at the 1-h PET scan. In addition, the ^{68}Ga-NOTA-AE105 PET scan clearly visualized metastatic spread to the ipsilateral axillary lymph nodes in both patients. This was confirmed with operative findings and final histopatohologic staging (Fig. 2). One of these patients (patient 6) was positive on the preoperative routine examination with ultrasound and fine-needle biopsies, whereas in the other patient (patient 1) the metastatic spread was found only during sentinel node operation and the following complete axillary lymph node dissection confirmed metastatic spread to 2 of 19 lymph nodes. Positive uPAR immunohistochemistry on surgical specimens of primary tumors and metastatic lymph nodes in both patients confirmed uPAR expression.

TABLE 3
Summary of uPAR PET/CT and Immunohistochemistry of uPAR Expression in Available Tumor Tissue

Patient no.	uPAR PET	Routine clinical CT/ operation/biopsy	10-min SUV_{mean}	10-min SUV_{max}	1-h SUV_{mean}	1-h SUV_{max}	uPAR histology
Primary tumor detection							
1	Breast	BC in biopsy and confirmed postoperatively	2.72	5.03	1.76	2.85	Positive
2	Prostate	PC in 12/12 biopsies	2.51	4.40	1.98	3.53	Positive
3	Prostate	PC in 12/12 biopsies	2.98	5.05	2.56	4.9	Positive
4	Prostate	PC in 12/12 biopsies	2.20	3.82	2.07	3.87	NA
5	Breast	BC in biopsy and confirmed postoperatively	2.52	3.83	2.26	3.86	Positive
6	0 urinary bladder lesions	No primary tumor on routine CT	NA	NA	NA	NA	NA
7	Prostate	PC 11/12 biopsies (2008)	2.26	4.63	1.32	2.52	NA
8	Prostate	No biopsies from primary tumor/no routine CT/ operation	1.82	3.74	1.23	2.69	NA
9	0 urinary bladder lesions	No primary tumor on routine CT	NA	NA	NA	NA	NA
10	Prostate	PC in 5/9 biopsies	2.22	4.76	0.69	2.20	Positive
Metastases detection							
1	2 axillary lymph node metastases	2 axillary lymph node metastases	2.56	3.41	1.53	2.08	Positive
2	No metastases	No lymph node metastases during staging operation	NA	NA	NA	NA	NA
3	No metastases	No lymph node metastases during staging operation	NA	NA	NA	NA	NA
4	No metastases	No lymph node metastases during staging operation	NA	NA	NA	NA	NA
5	2 axillary lymph node metastases	2 axillary lymph node metastases	2.10	2.75	1.09	2.71	Positive
6	No lesions	No residual disease on routine CT	NA	NA	NA	NA	NA
7	3 bone lesions	3 bone lesions on routine CT	1.86*	2.97*	1.22*	2.26*	NA
8	Multiple bone lesions	Multiple bone metastases on routine CT	3.60*	4.88*	1.71*	2.36*	NA
9	No uptake in 2 liver lesions	2 liver metastases on routine CT	NA	NA	NA	NA	NA
10	No metastases	No lymph node metastases during staging operation	NA	NA	NA	NA	NA

*Evaluation on 1 representative bone metastases.
NA = not applicable.
All primary prostate cancers showed heterogeneous physiologic tracer distribution, and SUVs are based on VOIs drawn using either CT tumor delineation or whole prostate gland.

PC

Of the 6 patients with PC, 4 patients with newly diagnosed locally advanced PC (patients 2, 3, 4, and 10) were included in the study before a planned open staging procedure with pelvic lymph node dissection. In these patients a low, heterogeneous intraprostatic distribution of the radioligand was found, with no distinct tumor uptake and no detectable tracer uptake in regional lymph nodes. The latter was in line with the findings at the open staging

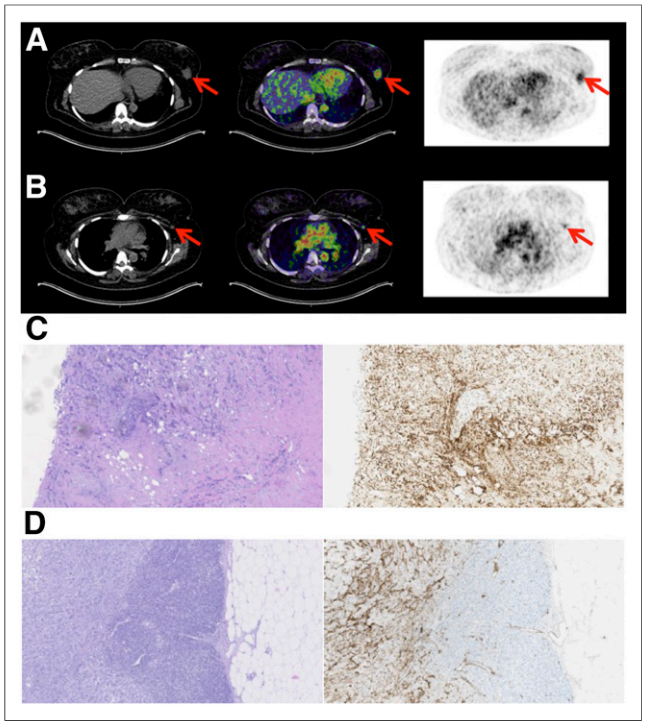

FIGURE 2. uPAR PET imaging in BC. (A) Representative transverse CT, PET, and coregistered PET/CT images of primary tumor lesion with intense uptake of ^{68}Ga-NOTA-AE105 (patient 1). (B) Images show uPAR-positive axillary lymph node metastasis (red arrow) with significant uptake in same patient. (C) Representative slides with intense uPAR immunohistochemistry staining and corresponding hematoxylin and eosin staining of tumor tissue from patient's primary tumor. (D) uPAR immunohistochemistry staining and corresponding hematoxylin and eosin staining of lymph node metastases.

procedure because pathologic examinations of the removed pelvic lymph nodes showed no lymph node involvement. The remaining 2 patients with PC (patients 7 and 8) had bone metastases and were evaluated before chemotherapy. Both patients had multiple metastases with significant ^{68}Ga-NOTA-AE105 uptake in several malignant lesions concurrent with heterogeneous uptake at the site of the primary tumor within the prostate gland. In the 3 available preoperative prostate biopsies, immunohistochemistry confirmed uPAR expression (Fig. 3).

UBC

Two patients with UBC were included in the study during an ongoing chemotherapy regime with only a small amount of residual disease. Both patients had proven response to chemotherapy, as evaluated by routine CT scans, before inclusion in the present study. In 1 patient (patient 9) there was no visible uptake of ^{68}Ga-NOTA-AE105 in 2 liver metastases, which were identified on the concomitant contrast-enhanced CT. No other lesions could be identified on either ^{68}Ga-NOTA-AE105 or diagnostic CT with intravenous contrast.

DISCUSSION

In this first-in-human study, we present the results of a ^{68}Ga-labeled uPAR PET radioligand, ^{68}Ga-NOTA-AE105. Together with our previous phase I study with the ^{64}Cu-labeled DOTA-AE105, the present study confirms that it is possible to detect uPAR expression in tumor lesions noninvasively with PET/CT.

uPAR PET/CT imaging with ^{68}Ga-NOTA-AE105 was safe, with no adverse events or obvious changes in general well-being or any vital signs. In addition, no significant changes in total blood count or kidney or hepatic function occurred.

As expected, the biodistribution analysis revealed the primary excretion route to be renal, with resulting high activity accumulation of ^{68}Ga-NOTA-AE105 in kidneys and urinary bladder due to the high hydrophilicity and small size of the peptide. In addition, a relatively high blood-pool activity could indicate some protein-bound activity of the intact ^{68}Ga-NOTA-AE105 or free ^{68}Ga bound to transferrin (*20*). The decreasing blood-pool activity argues against continuous transchelation of ^{68}Ga to transferrin, and the radioligand cleared fast from organs and the blood-pool activity probably reflects plasma protein bound activity. Compared with our ^{64}Cu-DOTA-AE105, we found a lower accumulation of activity in the liver after injection of ^{68}Ga-NOTA-AE105, which is favorable with respect to evaluation of possible liver metastases. Apart from the urinary tract, no other organ or tissues exhibited high nonspecific uptake of ^{68}Ga-NOTA-AE105.

The effective radiation dose was 0.0153 mSv/MBq, equaling 3.1 mSv at an injected activity of approximately 200 MBq, which was applied in the present study. This is lower or comparable to the radiation dose received from a standard ^{18}F-FDG PET scan, for which the effective dose is approximately 0.019 mSv/MBq, equal to 5.7 mSv at a standard dose of 300 MBq (*21*). The administration of intravenous contrast agent for the 1-h PET/CT scan could potentially result in a modest overestimation of SUVs in background organs. However, this is not expected to have any clinically significant effect on the calculated radiation dose, because

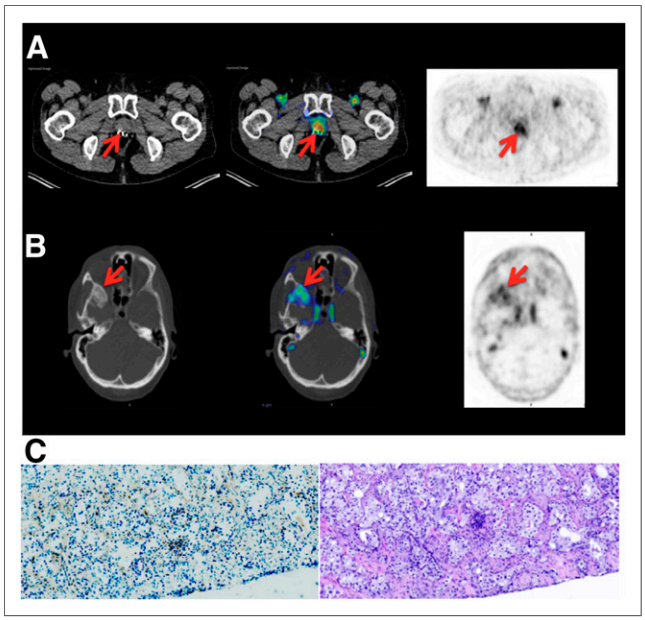

FIGURE 3. uPAR PET imaging in PC. (A) Representative transverse CT, PET, and coregistered PET/CT images with uptake of ^{68}Ga-NOTA-AE105 at site of primary tumor (patient 7). (B) Images show uPAR-positive metastasis in sphenoid bone (red arrow) with significant uptake in same patient. (C) Representative slides with weak uPAR immunohistochemistry staining of tumor tissue from preoperative biopsy and corresponding hematoxylin and eosin staining (patient 10).

based on our results from a previous study the average error in SUV_{mean} was found to be only 1.6% in background organs (*22*). In addition, it could be argued that a high tumor uptake potentially alters biodistribution. However, because the tumor burden in the current study was relatively small (localized PC, primary BC with no signs of spread, and UBC with minimal residual disease). We therefore believe that tumor uptake had no influence of the biodistribution and the final organ dosimetry.

Importantly, the radiation dose to bone marrow was below the recommended threshold value of 3 mSv (*23*) Therefore, the radiation burden of uPAR PET with ^{68}Ga-NOTA-AE105 is of no clinical concern, and the effective dose is comparable to that of other clinically applied ^{68}Ga-based PET radioligands, such as ^{68}Ga-labeled prostate-specific membrane antigen (*24*) and ^{68}Ga-DOTATATE/DOTATOC (*25*).

Plasma pharmacokinetic and urine metabolite analysis revealed intact ^{68}Ga-NOTA-AE105 in blood and urine and no formation of isotopic labeled metabolites, which is also found in other radioligands (*26,27*).

As a secondary objective of this phase I study, tumor detection, including SUVs and semiquantitative tumor uptake values, was evaluated. The radioligand performed well in the visual detection of metastatic tumor lesions, especially in BC, for which metastatic disease in ipsilateral axillary lymph nodes was found even in a situation in which the preoperative workup with ultrasound, fine-needle aspiration, and contrast-enhanced CT failed to detect the metastases. This is a clear clinical example of a potential future application of uPAR PET, because this patient could have gone directly to axillary lymph node dissection after uPAR PET and circumvented the other procedures if uPAR PET had been performed preoperatively. The current procedure with preoperative fine-needle biopsy finds only approximately one third of the patients with metastatic spread (*28*). Therefore, uPAR PET imaging could potentially be a superior technology for this purpose, when focusing on the high and specific radioligand uptake in lymph node metastases found in the present study. However, a sufficiently powered, controlled clinical trial has to be performed to prove this hypothesis.

The failure of ^{68}Ga-NOTA-AE105 PET to detect 2 metastases in the liver in a patient with disseminated UBC (patient 9) might question the application of ^{68}Ga-NOTA-AE105 for disseminated UBC. However, other PET radioligands, for example, 3′-deoxy-3′-^{18}F-fluorothymidine and ^{18}F-galacto-RGD, have also been reported to have lower activity in malignant liver lesions compared with the relatively high physiologic uptake in normal liver tissue (*29,30*). Another explanation could be downregulation of uPAR expression and tumor inactivation as a result of clinical response to chemotherapy before inclusion in the study. However, future studies to further investigate this hypothesis are warranted.

In PC and BC, tracer uptake in malignant tissue was visible on uPAR PET scans at 10 min and 1 h after injection. The optimal administered dose of ^{68}Ga-NOTA-AE105 and time for PET/CT scan after injection still needs to be established, but it is likely within the first 60 min, which is also the case for other peptide-based radioligands such as ^{68}Ga-prostate-specific membrane antigen (*24*), ^{68}Ga-DOTATATE/DOTATOC (*31*), and RGD peptides (*32*).

Histopathologic examination of the surgical specimens from the primary BC tumors/metastasis and the 3 available preoperative primary PC biopsies demonstrated uPAR expression in all patients, supporting target-specific uptake of ^{68}Ga-NOTA-AE105. Although the preoperative PC biopsies, compared with BC tissue, showed only weak uPAR expression, the limited number of patient samples made it impossible to apply a robust quantitative scoring system and no attempt was made to correlate ex vivo expression of uPAR in the excised surgical specimens with image-derived semiquantitative tracer uptake. It is possible that the general pattern of low, heterogeneous uptake of ^{68}Ga-NOTA-AE105 in prostatic tumors reflects weak tumor uPAR expression in these 6 PC patients who either had localized disease or were treated with radio-/chemotherapy. A significant correlation of uPAR expression based on immunohistochemistry and tumor uptake of the comparable radioligand ^{64}Cu-DOTA-AE105 has previously been demonstrated in murine tumor models (*12*). However, future prospective studies should ideally include a detailed and complete coregistration between imaging and subsequent cross-section pathology.

The artifact (halo effect) in the form of reduced activity around the urinary bladder with high physiologic activity uptake due to urinary excretion has been described using other ^{68}Ga-based ligands, such as ^{68}Ga-prostate-specific membrane antigen (*33*) and ^{68}Ga-DOTATOC (*34*). However, this is of no major concern because it is easily removed by prompt γ-correction, which will be implemented in future standard reconstruction algorithms for ^{68}Ga PET (oral personal communication with Siemens, November 2015).

In addition to BC staging, a promising application of a uPAR-based imaging agent may be in providing an imaging biomarker to determine the aggressiveness of a tumor, thereby giving prognostic information with possible therapeutic implications.

CONCLUSION

This first-in-human clinical study demonstrates the feasibility and potential of using a ^{68}Ga-labeled version of the AE105 peptide for uPAR-targeted PET imaging. The administration of ^{68}Ga-NOTA-AE105 was safe, was well tolerated, and provided satisfactory image contrast and identification of primary tumors and metastases. The most promising results were found in BC, with clear identification of metastatic axillary lymph nodes. Future phase II studies in larger patient populations with this indication will investigate the application and utility of uPAR PET in relevant clinical settings.

DISCLOSURE

This work was supported by the John and Birthe Meyer Foundation, the Danish National Advanced Technology Foundation, the Danish Council for Strategic Research, the Research Foundation of Rigshospitalet, the Capital Region of Denmark, the Novo Nordisk Foundation, the Lundbeck Foundation, the A.P. Moeller Foundation, the Svend Andersen Foundation, the Arvid Nilsson Foundation, Innovation Fund Denmark, and the Danish Council for independent research. Andreas Kjaer (AK), Morten Persson (MP), and Jacob Madsen (JM) are inventors of the composition of matter of uPAR PET with a filed patent application: Positron Emitting Radionuclides Labeled Peptides for Human uPAR PET Imaging (WO 2014086364 A1). AK, MP, and AK are cofounders of Curasight, which has licensed the uPAR PET patent to commercialize the uPAR PET technology (uTRACE®). Dorthe Skovgaard has received funding from Curasight. No other potential conflict of interest relevant to this article was reported.

ACKNOWLEDGMENTS

We thank all patients and their families for participating in this study. In addition, we will thank our excellent staff (Bente Dall, Susanne Svalling, Elisabeth Abrahamsson, and Maria Pejtersen) at the department for taking part in the conduction of the study.

REFERENCES

1. Dohn LH, Pappot H, Iversen BR, et al. uPAR Expression pattern in patients with urothelial carcinoma of the bladder: possible clinical implications. *PLoS One.* 2015;10:e0135824.
2. Grøndahl-Hansen J, Peters HA, van Putten WL, et al. Prognostic significance of the receptor for urokinase plasminogen activator in breast cancer. *Clin Cancer Res.* 1995;1:1079–1087.
3. Persson M, Kjaer A. Urokinase-type plasminogen activator receptor (uPAR) as a promising new imaging target: potential clinical applications. *Clin Physiol Funct Imaging.* 2013;33:329–337.
4. Persson M, Skovgaard D, Brandt-Larsen M, et al. First-in-human uPAR PET: imaging of cancer aggressiveness. *Theranostics.* 2015;5:1303–1316.
5. Jacobsen B, Ploug M. The urokinase receptor and its structural homologue C4.4A in human cancer: expression, prognosis and pharmacological inhibition. *Curr Med Chem.* 2008;15:2559–2573.
6. Danø K, Behrendt N, Høyer-Hansen G, et al. Plasminogen activation and cancer. *Thromb Haemost.* 2005;93:676–681.
7. Foekens JA, Peters HA, Look MP, et al. The urokinase system of plasminogen activation and prognosis in 2780 breast cancer patients. *Cancer Res.* 2000;60:636–643.
8. Riisbro R, Christensen IJ, Piironen T, et al. Prognostic significance of soluble urokinase plasminogen activator receptor in serum and cytosol of tumor tissue from patients with primary breast cancer. *Clin Cancer Res.* 2002;8:1132–1141.
9. Dohn LH, Illemann M, Høyer-Hansen G, et al. Urokinase-type plasminogen activator receptor (uPAR) expression is associated with T-stage and survival in urothelial carcinoma of the bladder. *Urol Oncol.* 2015;33:165.e15–24.
10. Almasi CE, Brasso K, Iversen P, et al. Prognostic and predictive value of intact and cleaved forms of the urokinase plasminogen activator receptor in metastatic prostate cancer. *Prostate.* 2011;71:899–907.
11. Almasi CE, Christensen IJ, Høyer-Hansen G, et al. Urokinase receptor forms in serum from non-small cell lung cancer patients: relation to prognosis. *Lung Cancer.* 2011;74:510–515.
12. Persson M, Madsen J, Østergaard S, et al. Quantitative PET of human urokinase-type plasminogen activator receptor with ^{64}Cu-DOTA-AE105: implications for visualizing cancer invasion. *J Nucl Med.* 2012;53:138–145.
13. Persson M, Madsen J, Østergaard S, Ploug M, Kjaer A. ^{68}Ga-labeling and in vivo evaluation of a uPAR binding DOTA- and NODAGA-conjugated peptide for PET imaging of invasive cancers. *Nucl Med Biol.* 2012;39:560–569.
14. Persson M, Hosseini M, Madsen J, et al. Improved PET imaging of uPAR expression using new ^{64}Cu-labeled cross-bridged peptide ligands: comparative in vitro and in vivo studies. *Theranostics.* 2013;3:618–632.
15. Persson M, Liu H, Madsen J, Cheng Z, Kjaer A. First ^{18}F-labeled ligand for PET imaging of uPAR: in vivo studies in human prostate cancer xenografts. *Nucl Med Biol.* 2013;40:618–624.
16. Persson M, El Ali HH, Binderup T, et al. Dosimetry of ^{64}Cu-DOTA-AE105, a PET tracer for uPAR imaging. *Nucl Med Biol.* 2014;41:290–295.
17. Persson M, Nedergaard MK, Brandt-Larsen M, et al. Urokinase-type plasminogen activator receptor as a potential PET biomarker in glioblastoma. *J Nucl Med.* 2016;57:272–278.
18. Velikyan I. Prospective of ^{68}Ga-radiopharmaceutical development. *Theranostics.* 2013;4:47–80.
19. Hong I, Rothfuss H, Furst S, Casey M. Prompt gamma correction for Ga-68 PSMA PET studies. *IEEE Nucl Sci Symp Med Imaging Conf Rec.* 2015.
20. Roesch F, Riss PJ. The renaissance of the Ge/Ga radionuclide generator initiates new developments in Ga radiopharmaceutical chemistry. *Curr Top Med Chem.* 2010;10:1633–1668.
21. Deloar HM, Fujiwara T, Shidahara M, et al. Estimation of absorbed dose for 2-[F-18]fluoro-2-deoxy-D-glucose using whole-body positron emission tomography and magnetic resonance imaging. *Eur J Nucl Med.* 1998;25:565–574.
22. Berthelsen AK, Holm S, Loft A, Klausen TL, Andersen F, Højgaard L. PET/CT with intravenous contrast can be used for PET attenuation correction in cancer patients. *Eur J Nucl Med Mol Imaging.* 2005;32:1167–1175.
23. International Atomic Energy Agency. *Strategies for Clinical Implementation and Quality Management of PET Tracers.* Vienna, Austria: International Atomic Energy Agency; 2009.
24. Herrmann K, Bluemel C, Weineisen M, et al. Biodistribution and radiation dosimetry for a probe targeting prostate-specific membrane antigen for imaging and therapy. *J Nucl Med.* 2015;56:855–861.
25. Sandström M, Velikyan I, Garske-Román U, et al. Comparative biodistribution and radiation dosimetry of ^{68}Ga-DOTATOC and ^{68}Ga-DOTATATE in patients with neuroendocrine tumors. *J Nucl Med.* 2013;54:1755–1759.
26. Szabo Z, Mena E, Rowe SP, et al. Initial evaluation of [^{18}F]DCFPyL for prostate-specific membrane antigen (PSMA)-targeted PET imaging of prostate cancer. *Mol Imaging Biol.* 2015;17:565–574.
27. Hofmann M, Maecke H, Börner R, et al. Biokinetics and imaging with the somatostatin receptor PET radioligand ^{68}Ga-DOTATOC: preliminary data. *Eur J Nucl Med.* 2001;28:1751–1757.
28. Cools-Lartigue J, Meterissian S. Accuracy of axillary ultrasound in the diagnosis of nodal metastasis in invasive breast cancer: a review. *World J Surg.* 2012;36:46–54.
29. Beer AJ, Schwaiger M. *Molecular Imaging: Methods and Protocols.* New York, NY: Springer; 2011:183–198.
30. Barwick T, Bencherif B, Mountz JM, Avril N. Molecular PET and PET/CT imaging of tumour cell proliferation using F-18 fluoro-L-thymidine: a comprehensive evaluation. *Nucl Med Commun.* 2009;30:908–917.
31. Velikyan I, Sundin A, Sörensen J, et al. Quantitative and qualitative intrapatient comparison of ^{68}Ga-DOTATOC and ^{68}Ga-DOTATATE: net uptake rate for accurate quantification. *J Nucl Med.* 2014;55:204–210.
32. Iagaru A, Mosci C, Shen B, et al. ^{18}F-FPPRGD2 PET/CT: pilot phase evaluation of breast cancer patients. *Radiology.* 2014;273:549–559.
33. Afshar-Oromieh A, Haberkorn U, Schlemmer HP, et al. Comparison of PET/CT and PET/MRI hybrid systems using a ^{68}Ga-labelled PSMA ligand for the diagnosis of recurrent prostate cancer: initial experience. *Eur J Nucl Med Mol Imaging.* 2014;41:887–897.
34. Gaertner FC, Beer AJ, Souvatzoglou M, et al. Evaluation of feasibility and image quality of ^{68}Ga-DOTATOC positron emission tomography/magnetic resonance in comparison with positron emission tomography/computed tomography in patients with neuroendocrine tumors. *Invest Radiol.* 2013;48:263–272.